Power generation based on the $Ca(OH)_2$/ CaO thermochemical storage system – experimental investigation of discharge operation modes in lab scale and corresponding conceptual process design

Matthias Schmidt[1], Marc Linder[1]

[1]German Aerospace Center – DLR e.V., Institute of Engineering Thermodynamics, Linder Höhe, 51147 Köln, Germany

Corresponding author: Matthias Schmidt, Matthias.schmidt@dlr.de

Highlights

Experimental investigation of thermal discharging in a lab scale reactor

Operation of storage system at 4 – 470 kPa and temperatures of 280 °C – 600 °C

Demonstration of operation modes at boundary conditions to drive a Rankine cycle

Analysis of power generation with CaO and water and assessment of storage efficiency

keywords: thermochemical energy storage; calcium hydroxide/ oxide; thermal discharge operation modes; high vapor pressures; power generation; storage efficiency

Abstract

Thermochemical storage systems offer in theory promising advantages for a wide range of applications. In particular the reversible reaction of calcium hydroxide to calcium oxide and water vapour is intensively discussed as an alternative storage solution for concentrated solar power plants. The material is cheap, environmentally friendly and discharge temperatures of the reaction of 600 °C and above fit to the operating range of today´s power plants. However, experimental data on the operation of the system in lab scale and at load conditions comparable to the real application is rarely reported.

Therefore the thermal discharge of the reaction system at vapour pressures between 4 and 470 kPa and temperatures between 280 – 600 °C is experimentally investigated in this study. In particular the influence of the cooling load at various vapour pressures on the achievable discharge temperatures is analysed. The presented data complements the experimental characterisation of the reaction system in the complete temperature and pressure range which is relevant for real process applications. Based on this knowledge the applicability of the storage for various processes can now be assessed more accurate. By means of the experimental results a first integration option of the thermochemical system in a CSP plant is proposed in this work and thermodynamically analysed. The analysis revealed that, when the required steam production during discharge is thermally integrated into the Rankine steam cycle, a high storage efficiency of up to 87 % can be reached compared to only 60 % in the reference case.

1 Introduction

Concentrating solar power (CSP) plants can produce electricity completely renewable and free of carbon dioxide emissions. Since this technology converts solar irradiation into thermal energy in the first step a combination with large scale thermal energy storage system allows the decoupling of the availability of solar energy from the electricity production.

Until today, the parabolic through technology is the most advanced, with the greatest number of commercial plants in operation [1]. However the central receiver tower technology with molten salt as heat transfer fluid is gaining importance because they operate at higher maximum temperatures of currently 565 °C and the molten salt can directly be stored in large tanks with minimal losses [2,3]. Large molten salt tower plants like the Gemasolar (20 MWe and 15 hours storage) in Spain or the Cresecent Dunes plant (110 MWe and 10 hours storage) in the US have been recently set into operation and more plants based on this technology are currently under development.

The direct two tank molten salt system is the state of the art storage system for today's CSP plants. Nevertheless in a typical configuration the salt itself accounts for around 50 % of the cost of the storage system [4]. In order to reduce the costs researchers investigate alternative thermal storage solutions [5]. In the thermocline concept for example the expensive salt is partly replaced with inexpensive filler materials and only one storage tank is used [6]. Besides these approaches for cost reduction in sensible storage systems also latent [7–9] and thermochemical systems are gaining importance. Recently published review articles give a comprehensive overview of high temperature thermal storage technologies,their state of development and potential applications [10–14]..

Among the thermal energy storage methods thermochemical systems offer in theory a very promising potential [15,16]. Some of the reaction systems have high energy densities, the storage principal itself is free of losses and especially the temperature at which the heat is released can be adjusted in a certain range [17,18]. A very recent survey of thermochemical storage technologies and their level of maturity is given by Pardo et al. [19] and Prieto et al. [20].

One reaction system suggested for CSP applications is the reversible reaction of calcium hydroxide to calcium oxide and water vapour. First of all, the material is very cheap and abundantly available in industrial scale. Combined with the high enthalpy of reaction the material offers in principle a very cheap storage capacity. Secondly the theoretical temperature range of the reaction between 300 °C and up to 600 °C fits to the operating range of the plant. Thirdly, the gaseous reactant, water vapour, can safely be handled and stored volume efficient as liquid water.

Despite these advantages the technology development is still in an early research state. The majority of the works focus on investigations with small sample masses in thermogravimetric apparatus. Cycle stability has first been proven by Rosemary for 1171 cycles [21]. Kinetic equations for the de- and rehydration have been derived by several authors [22–24] and the development of simulation models is still ongoing [25,26]. Other groups focus on the modification of the material in order to enhance the reaction rate [27], adapt the reaction temperatures [28], or to encapsulate the storage material in a permeable shell [29]. These investigations on the material level are important to improve the fundamental understanding of the reaction system. But for the development of a thermochemical storage systems additional experimental research in larger reactors and under process relevant boundary conditions is essential.

In lab and pilot scale set-ups two different type of reactor concepts are currently realized. One is the so called directly heated concept where the heat transfer fluid is in direct contact with the reacting particles. Pardo et al. carried out the reaction in a fluidized bed for 1.9 kg of material composed of 30 %w $Ca(OH)_2$ and 70 %w inert easy to fluidize particles [30]. Criado et al. presented a theoretical study on a fluidized bed concept for large CSP plants [31] while recently the group proofed the concept experimentally in a newly constructed lab scale set up [32].

The second concept is the so called indirectly heated reactor where the heat transfer fluid is physically separated from the storage material and the thermal energy is transferred via a heat exchanging surface. Experimental data on the operation of indirectly heated reactors is rather scarce. Ogura et al. firstly presented a reactor where heat from the exothermal reaction was transferred to an air flow at ambient temperature [33] and Yan et al. performed the exothermal reaction at different vapour pressures but the reactor did not allow the recovery of the released heat [34]. Even though these investigations are helpful to understand the reaction in larger scale, the experiments do not sufficiently represent the required operation modes of an indirectly heated storage system in the real application. In case of thermal energy storage both the endo- and exothermal reaction will be thermally driven by the heat transfer fluid and the reaction system has to be operated in a pressure and temperature range which depends on the boundary conditions of the process only.

Figure 1 shows the theoretical equilibrium line of the reaction calculated by values from Barin [35] as well as the upper and lower temperature limit of current molten salt tower plants (red dashed lines). The relevant operating range for the indirectly heated storage system is marked as grey area. In a recent publication of our group we analysed the thermal charging of the system at different low vapour pressures in detail [36] (dehydration conditions marked with partly filled red squares). The present study therefore focuses in the first part on the discharge reaction at different pressures between 4 and up to 470 kPa at different cooling loads (operating conditions marked with blue triangles). The presented data complements our experimental characterisation of the reaction system in the complete temperature and pressure range which is relevant for real process applications. Based on the experimental results a first integration concept of the storage system into a CSP plant has been analysed theoretically in the second part of the paper with a special focus on the operation of the power block with the storage system as the only energy source. For this application case we analysed how the use of different low grade heat sources from the Rankine cycle to evaporate steam for the discharge reaction affects the overall storage efficiency. The charging performance has been assessed taking the available condensation temperature at the plant location as well as the experimentally determined operation characteristic into account.

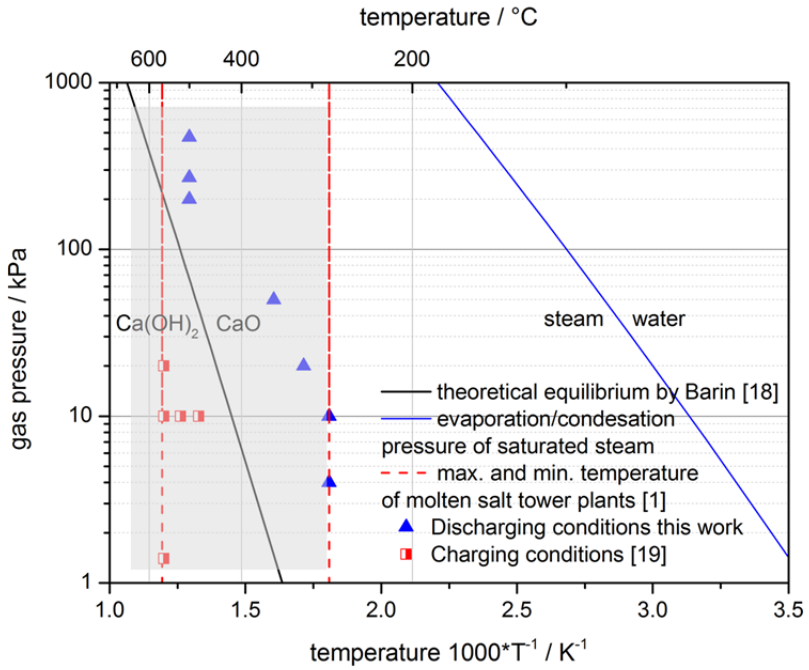

Fig. 1 Equilibrium line of the reaction system $Ca(OH)_2/CaO$ and operating temperature range of molten salt; experimental conditions of the presented experiments in this work

2 Experimental set up

2.1 Reactor

The reactor used in this study was especially designed to analyse the thermal capability of the reaction system in operation modes and boundary conditions comparable to the operation in the real application. This on one hand means that the reaction is driven by indirect heating or cooling loads induced by the heat transfer fluid and on the other hand the reaction gas is supplied or removed through a comparable system and within the respective pressure range. An additional approach was to minimize heat and mass transport limitations which in general are contributed to the reactor design, in order to characterise the operational performance of the commercial calcium hydroxide material. For more details on the reactor please refer to our previous publication [36].

Figure 2 left shows the reactor which consists of one single heat exchanger plate. Air serves as the heat transfer fluid in the experimental set up and flows inside the plate while a bulk of reactive material (white powder in Fig. 2 left) is placed on both sides of the plate. The inside area of the plate is 1600 mm long, 150 mm wide and surrounded by a frame of 10 mm height. In this volume of 2.4 L on each side of the plate the storage material can be placed. The total heat exchange surface is 0.48 m². The reaction bed is encased with a gas permeable metallic filter (pore size 5 µm) to hold the reaction bed in position (Figure 2 right).

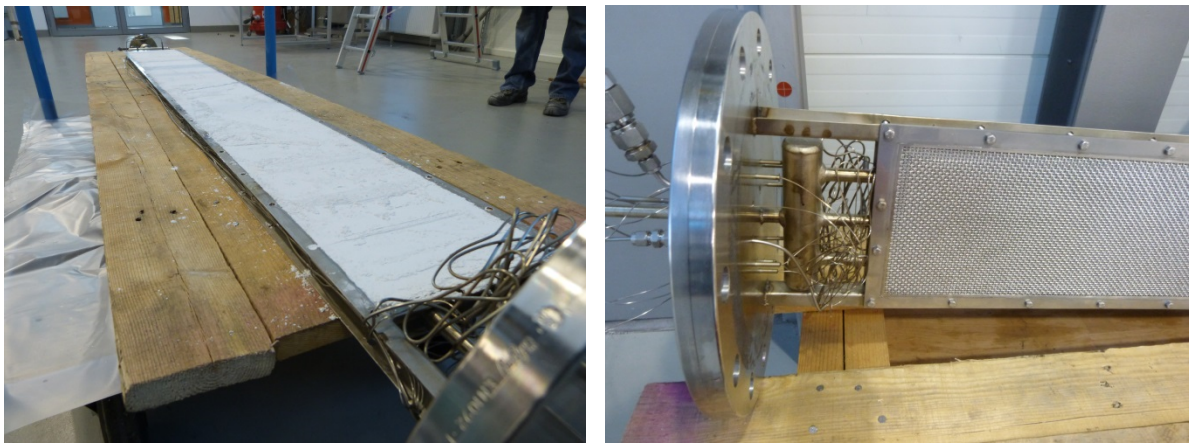

Fig. 2 left: heat exchanger plate filled with calcium hydroxide; right: reaction bed encased with gas permeable metal filter plate

The heat exchanger plate with the encased reaction bed is placed into a casing pipe of 200 mm in diameter. The casing pipe is made of stainless steel (alloy 1.4571) with a wall thickness of 3 mm in order to operate at pressures of up to 1000 kPa and 550 °C. Figure 3 right shows a sectional view of the reaction bed in the casing pipe including important dimensions and positions of measurement instruments. To record the air inlet ($\vartheta_{Air,in}$) and outlet temperature ($\vartheta_{Air,out}$) a thermocouple is placed directly before and after the reaction bed. Seven thermocouples $\vartheta_{1\text{-}7}$ (type K, ± 0.4 % X T) measure the material temperature in the reaction bed. These are positioned 5 mm in vertical distance from the heat exchange surface and every 200 mm along the horizontal direction of the air flow. An additional pressure sensor (p_1) (PPA-35XHTT, Keller Ges. für Druckmesstechnik mbH, ± 0.8 kPa) mounted into the casing, records the vapour pressure in the reaction chamber.

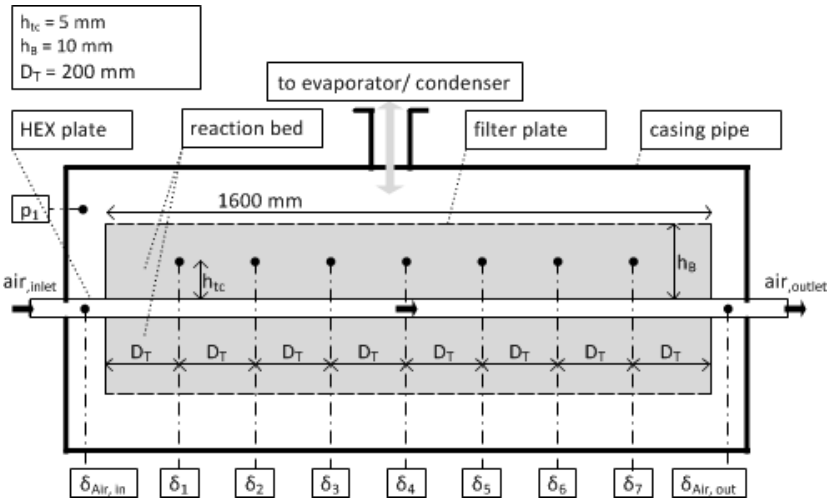

Fig. 3 sectional view of the reaction bed in the casing pipe including important dimensions and position of measurement instruments

2.2 Material

In total 2.4 kg of $Ca(OH)_2$, supplied by Rheinkalk GmbH / Lhoist group (product type "Sorbacal©H"), has been filled into the reactor. According to the companies data sheet the d_{50} is 5.5 µm and the purity of the material is 97 - 98 %.

2.3 Experimental procedure

The reactor is integrated into an infrastructure which supplies the heat transfer fluid and handles the reaction gas. A flow sheet and a more detailed description of the test bench can also be found in a previous publication on this set up [36]. Air, supplied by a compressor, serves as the heat transfer fluid. The air volume flow is adjusted by a mass flow controller (Bronkhorst, digital flow controller, ± 0.4 %) before it gets heated up with an electrical preheater and enters the reactor. To supply the reaction gas, the central outlet of the casing pipe (compare Fig. 3) is connected to the evaporator. The evaporator consists of a tube bundle heat exchanger where the shell side is partly filled with liquid water (for evaporation) and thermal oil runs on the tube side. By tempering the inlet temperature of the thermal oil with a thermostatic bath an evaporation pressure between 0.7 and 618 kPa can be adjusted. A filling level meter (Vegaflex 65, ± 2 mm) records the change of the water level in the evaporator. By means of this value the conversion of the storage material is determined.

Before every discharge experiment the material present in the reaction bed is completely dehydrated and the whole set up is evacuated with the vacuum pump ensuring a pure water vapour atmosphere during the experiment. Afterwards the valve to the evaporator is closed. The air flow is started and set to a certain preheating temperature. Additionally the auxiliary heating cables attached to the casing pipe to minimize thermal losses are set to the same preheating temperature. Simultaneously the evaporation pressure for the experiment is adjusted. When the vapour pressure and the temperatures in the reaction bed become constant the experiment can be started by opening the valve between evaporator and reactor. Consequently the pressure in the reactor increases and the exothermal reaction takes place. The heat released by the reaction is taken up from the heat transfer fluid. When the heat of reaction is completely released and the temperatures in the bed reach their initial values again the experiment is finished. The operation parameters of all experiments are given in table 1.

We already published a detailed investigation of the charging procedure with the same reactor [36].

Therefore dehydration experiments are not presented in this study. However, the dehydration reaction after every discharge experiment of this study was performed at identical conditions (air temperature of 500 °C and a condensation pressure of 10 kPa in the condenser). The experiments A to E are part of a measurement series where one batch of the material (described in 2.2) was cycled for 10 times in total. The experiments F to I are part of a second measurement series (35 cycles in total) performed with another batch of the same starting material. The respective cycle number for each experiment is given in Table1.

Table 1 *Parameters of all experiments presented in this study*

Experiment	$T_{air,\ initial}$ / °C	$\dot{V}$ / $\frac{Nm^3}{h}$	$p_{evaporator}$ / kPa	T_{water} / °C	Cycle No.
Hydration					
A	500	16	470	150	5
B	500	20	470	150	4
C	500	28	470	150	7
D	500	20	200	45	2
E	500	20	270	60	3
F	280	12	4	32	21
G	280	12	10	45	32
H	310	12	20	60	9
I	350	12	50	81	10

3 Experimental results and discussion

3.1 Thermal discharging at 200-470 kPa

In a real application the storage system should ideally supply thermal energy at an as high as possible temperature level in order to reach for example high efficiencies in the power block. Therefore we performed the discharging procedure at high vapour pressures and evaluated the capability of the reaction system to supply thermal energy at temperatures between 500 – 600 °C.

Figure 4 shows the reference discharge experiment A. The reaction bed is preheated to a temperature of 500 °C while in the evaporator a temperature of 150 °C is adjusted (for all parameters refer to experiment A in Table1). At minute 0 the valve between evaporator and reactor is opened thus the pressure in the reactor increases up to 470 kPa (red dash dotted line). Triggered by the pressure increase the exothermal reaction set in and the material temperatures in the front (ϑ_1), middle (ϑ_3) and rear (ϑ_7) of the reaction bed jump to a maximum of 600 °C. The reached temperature corresponds to the equilibrium temperature (grey dashed line) which was calculated with the measured pressure in the reactor and the correlation given by Samms et al. [37]. Furthermore, we observe a clear reaction front in the horizontal direction of the air flow. At all three measurement points the reaction proceeds very close to the equilibrium temperature which is indicated by the constant temperatures plateaus and the simultaneously measured constant increase in conversion. The temperature (ϑ_1) drops after 8 minutes which indicates that a major part of the material in the front region is already completely converted. The reactive area then moves along the reaction bed until also the material in the rear region has completely reacted and (ϑ_7) starts to decreases after 35 minutes. Accordingly 80 % of the total mass is converted after 35 minutes (black cross dots) while a total conversion of 92 % is measured after 60 minutes.

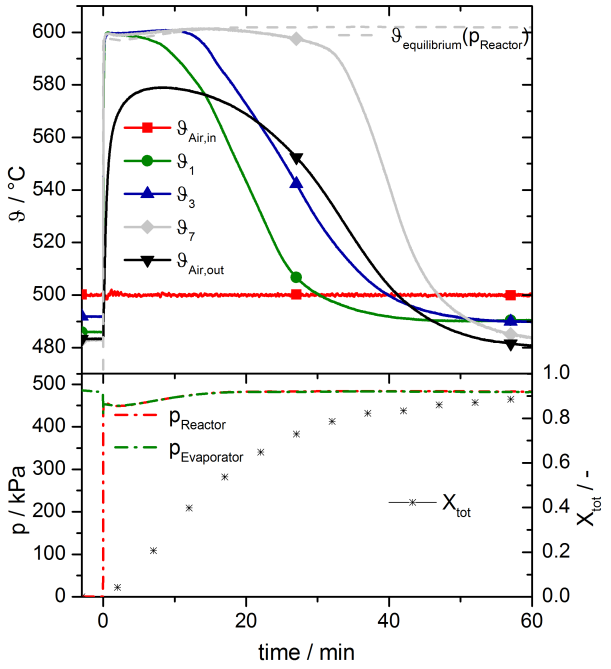

Fig. 4 Hydration experiment at 470 kPa and a starting temperature of 500 °C

Variation of cooling load at 470 kPa

In order to analyse the thermal capability of the reaction system at 470 kPa, experiments with three different cooling loads have been performed. Experiment A was conducted with an air volume flow of 16 Nm³/h while the volume flow was increased to 20 and 28 Nm³/h for the experiments B and C respectively. For all cases a constant air inlet temperature of 500 °C and an evaporation temperature of 150 °C was adjusted (refer to table 1 for details of the experimental conditions). Figure 5 shows the temperature trends in the front (ϑ_2) and rear (ϑ_6) region of the reaction bed as well as the air outlet temperature. We can observe that the reaction proceeds at a constant temperature which corresponds to the theoretical equilibrium temperature (dashed lines). The lengths of the plateaus directly correlate to the applied cooling loads. With an increasing cooling load (experiment A to B to C) the plateaus become shorter which can be attributed to a faster conversion. It is remarkable that even at a more than 40 % higher cooling load (compare A to C) no deviation of the plateau temperature from the equilibrium temperature can be observed. This indicates that the heat released by the exothermal reaction keeps up with the heat removed out of the reaction bed for all applied cooling loads. In other words the reaction rate is controlled by the heat transport out of the reaction bed. It can be concluded that at a pressure of 470 kPa the reaction is very fast even at (very close to) the equilibrium temperature.

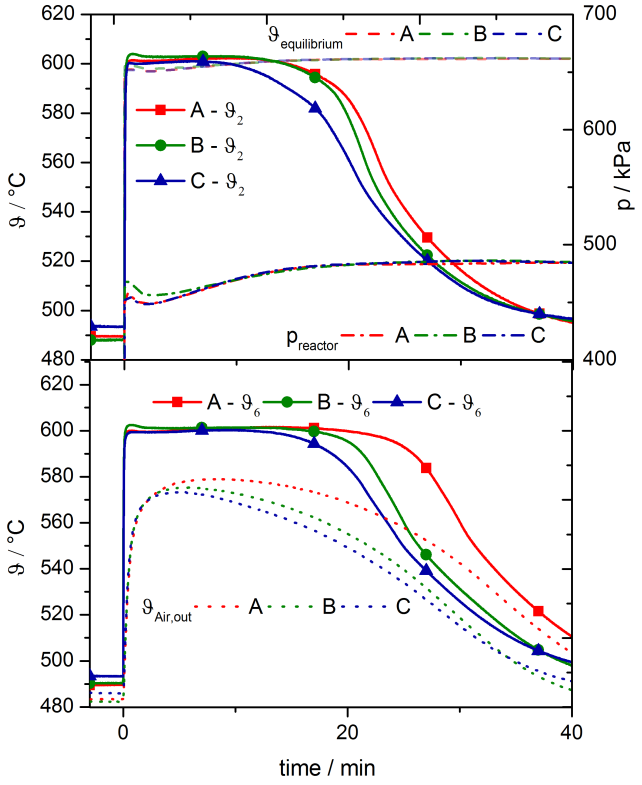

Fig. 5 Hydration at 470 kPa and a starting temperature of 500 °C under different cooling loads

Variation of discharge pressure

Even though the discharge of the storage system at 470 kPa showed good performance, it might be reasonable to operate the system at slightly lower vapour pressures depending on the boundary conditions of the process. For example if the available heat source for evaporation has a lower temperature level than 150 °C. Therefore and to complete the operating range between 500 and 600 °C we conducted additional discharge procedures at 200 and 270 kPa (experiment D and E). The reactor again was operated at a constant air flow rate of 20 Nm³/h and an air inlet temperature of 500 °C.

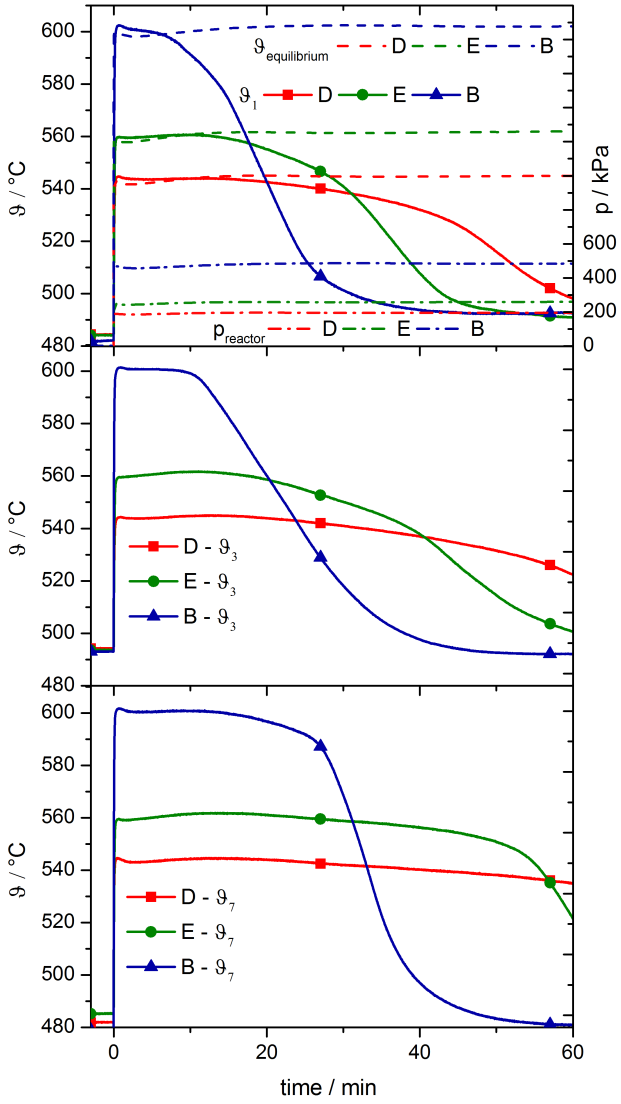

Fig. 6 Hydration experiment at 200, 270 and 470 kPa and a starting temperature of 500 °C

Figure 6 shows the temperature trends of ϑ_1 (beginning of the reaction bed), ϑ_3 (middle of the reaction bed) and ϑ_7 (end of the reaction bed) for the experiments D and E as well as for comparison the experiment B with a pressure of 470 kPa. We can see that in all cases the reached maximum temperature corresponds to the predicted temperature by the equilibrium line. The small differences within the first minutes can be contributed to pressure differences between the global measured pressure in the casing pipe and the pressure in the reaction bed (compare position of pressure sensor in Fig. 3) which occur during the initial dynamic changes. Consistently in all experiments a reaction front moves along the direction of the air flow. Close to the air inlet where initially the cooling load is the highest, the material temperatures (ϑ_1) drop at first due to a decreasing amount of reacting material. The plateaus in the middle region (ϑ_3) are longer while the temperatures in the rear region drop at last.

The cooling loads of the experiments also vary due to the different temperature differences between the air inlet temperature and the plateau temperatures. Accordingly the experiment with the highest plateau temperature (case B) is the first where the heat released by the reaction is completely

absorbed and all reaction bed temperatures reach their initial values again (after 60 minutes at ϑ_7). With lower cooling loads (induced due to lower vapour pressures), in the cases D and E, the duration of the discharge procedure prolongs (timeline is not plotted until the end of the experiments D and E).

3.2 Thermal discharging at 4 – 50 kPa

Discharge at 4 kPa

Figure 7 shows the temperature and conversion trend within the first 30 minutes of the discharge experiment at a vapour pressure of 4 kPa. The reaction bed is preheated with an air flow rate of 12 Nm³/h at an inlet temperature of 280 °C (red solid line). The reaction chamber is evacuated while the evaporator is adjusted to a temperature of 30 °C. At minute zero the valve between reactor and evaporator is opened indicated by the pressure increase in the reactor (red dash dotted line). Correspondingly the material temperatures rise quickly due to the heat released by the exothermal reaction. A particular important observation is that temperature plateaus arise at different levels according to the positions in the reactor. The temperature plateaus indicate an equilibrium state between the heat released by the reaction and the heat absorbed by the heat transfer fluid. Coherently we observe the lowest plateau temperature of 340 °C in the front region (ϑ_1) of the reactor, where the cooling load is maximal due to the proximity to the air inlet. Smaller cooling loads in the middle (ϑ_5) and rear (ϑ_7) region of the reactor lead to higher plateau temperatures of approximately 350 °C (ϑ_5) and 360 °C (ϑ_7). This correlation can directly be ascribed to the dependency of the reaction rate from the temperature gap to the equilibrium. With an increasing distance between reaction temperature and equilibrium temperature the rate of reaction increases. The temperature plateaus of the experiment reveal that at a pressure of 4 kPa a certain gap to the equilibrium needs to be maintained in order to operate at high cooling loads. This is in contrast to the reference experiment at 470 kPa where the storage system could be operated at the equilibrium temperature even at drastically increased cooling loads. However it can be stated that the discharging with a vapour pressure of 4 kPa is possible and an outlet temperature of 340 °C, 25 K lower than the equilibrium temperature, can be expected with reasonable cooling rates. It has to be mentioned that the trend lines in Fig. 7 are not presented until the end of the experiment in order to focus on the temperature plateaus. The reaction was completed after 140 minutes.

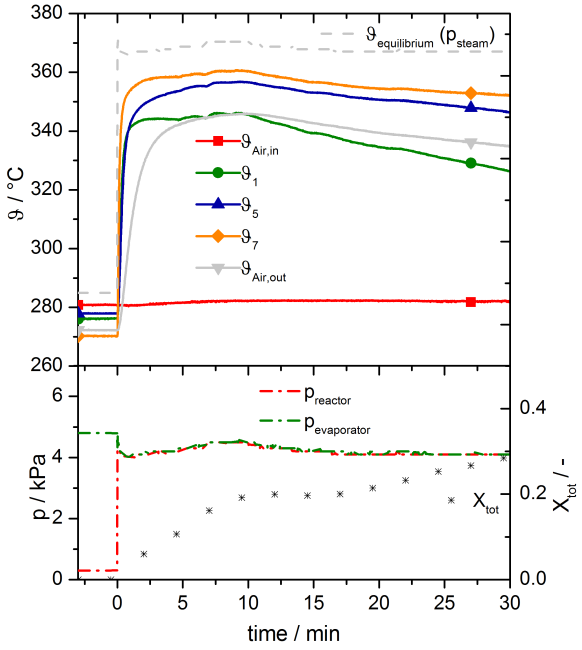

Fig. 7 Hydration at 4 kPa and a starting temperature of 280 °C

Discharge at 10 kPa

The discharge of the storage system at a pressure of 10 kPa is of particular interest since in many process applications low grade heat at a temperature level of 45 °C, which can be used to generate steam at 10 kPa, is available. The hydration experiment is performed at a volume flow of 12 Nm³/h, a starting temperature of 280 °C and an evaporation temperature of 45 °C. Figure 8 shows the temperature and conversion trend for the first 30 minutes after the exothermal reaction is triggered by the pressure increase in the reactor. Complete conversion was reached after 100 minutes in this experiment (timeline in Fig. 8 is shortened in order to focus the display on the temperature plateaus). A qualitatively similar temperature trend compared to the experiment at 4 kPa can be observed. Temperature plateaus arise at different levels according to the different cooling loads in the front (ϑ_1), middle (ϑ_5) and rear (ϑ_7) part of the reaction bed. The temperature plateau in the front region where the highest cooling load applies arises at 360 °C for these experimental conditions. Consequently for the real application it can be derived that at a discharge pressure of 10 kPa an additional temperature distance to the theoretical equilibrium temperature must be maintained to allow the operation with high cooling loads.

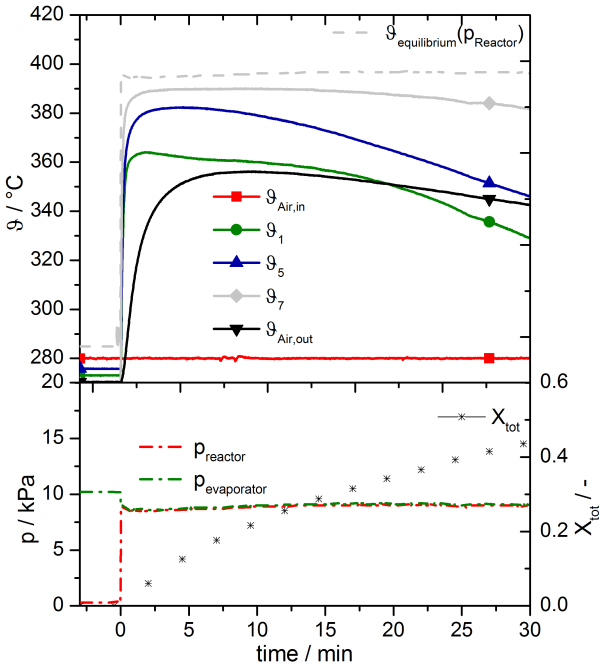

Fig. 8 Hydration at 10 kPa and a starting temperature of 280 °C

Variation of discharge pressure

Since the temperature level of the available heat source for evaporation depends on the process of the real application we additionally analysed the discharge operation at vapour pressures of 10, 20 and 50 kPa, respectively at evaporation temperatures of 45 °C, 60 °C and 81 °C. The air volume flow was 12 Nm³/h for all experiments while the air inlet temperature is constant but different for each case in order to achieve comparable cooling loads. The air inlet temperature and starting temperature in each experiment is set 120 K lower than the theoretical equilibrium temperature at the applied vapour pressure. For example, experiment F was operated at a water vapour pressure of 50 kPa which correspond to an equilibrium temperature of 470°C. Therefore the air inlet temperature was set to 350 °C. For comparison of the experimental parameters please refer to Table 1.

As already explained the cooling load is initially maximal in the front region of the reactor. Figure 9 therefore only represents the temperature ϑ_1 (beginning of reaction bed) and the equilibrium temperature based on the measured pressure for each experiment. It can clearly be observed that in all cases plateaus arises while a certain gap to the equilibrium temperature is maintained. The gap is about 15 K for case H and I (50 and 20 kPa respectively) while it is approximately 30 K for the cases F and G (4 and 10 kPa).

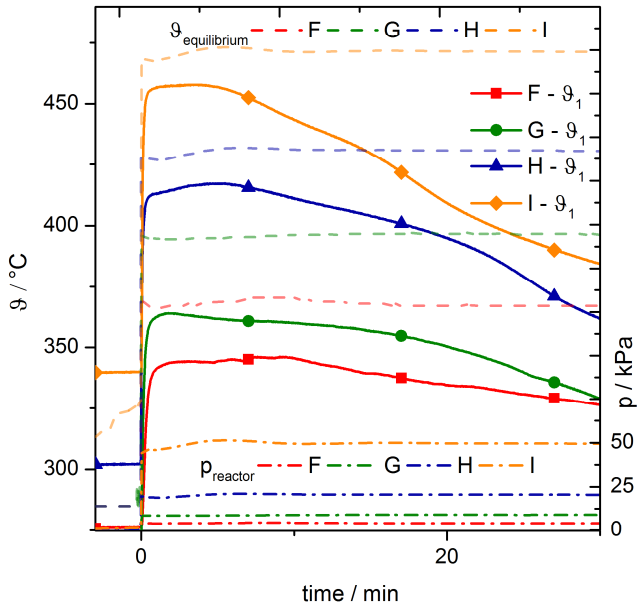

Fig. 9 Hydration at 4, 10, 20 and 50 kPa under comparable cooling loads

3.3 Cycle stability and changes of the reaction bed

Cycle stability of the reaction system has already been demonstrated in several works by means of TGA as well as reactor experiments. Therefore the analysis of the cycle stability was not a main focus of this study. Nevertheless we can confirm that for the performed experiments in general a conversion of 90-95 % (compare Fig. 4 and the experiments presented in [36]) was achieved and no decreasing tendency over the number of cycles could be observed. As already mentioned the conversion of the experiments in Figure 7 and Figure 8 do not show complete conversion because the timeline is not presented until the end of the experiment (to improve the display of the discussed temperature plateaus). That the conversion reaches only 90-95 % in the lab scale reactor can be attributed to two reasons. First is, that the purity of the basic raw material is only 97-98 % $Ca(OH)_2$. The second reason is that the last 5-10 % of conversion during the dehydration demands a very long time. Since full conversion of the material does not have any influence on the phenomena's discussed in this paper, experiments were finished when a conversion between 90 – 95°% was reached. Overall we can confirm that the reaction is cycle stable and 90°% of the theoretical full conversion is exploitable in technically relevant times.

The right picture in Figure 10 shows the reaction bed of $Ca(OH)_2$ when it was removed from the casing pipe after 35 cycles. It can be observed that the reaction bed is slightly compressed and the bulk density increased compared to the initially loose filling (compare Fig. 2) of the storage material. Roughly 20 % of the heat exchange surface is not covered with material anymore due to the compression of the bed. The compression might enhance the thermal conductivity of the bulk on the one hand but could also worsen the gas permeability on the other hand. We assume that these changes occur within the first cycles and subsequently do not significantly change anymore. In addition no effect dedicated to these changes of the reaction bed could be observed in our experiments. However the reaction bed design (very thin layer) also was explicitly dedicated to minimize these transport resistances. Nevertheless the findings indicate that in larger reactors the

changes which occur in large reactive bulks might have a significant influence on the performance. The heat and mass transport phenomena's in a changing reactive bulk should therefore be investigated in an experimental set up especially designed to address these questions. A more detailed description of these transactions in the models will improve simulation results. The picture in Figure 10 left shows the agglomerates after loosening of the bulk but even though the agglomerates look very hard, they fall apart into smaller particles with only slight mechanical strains. This formation of agglomerates has consistently been reported in lab scale reactors, even in the directly heated fixed bed.

Fig. 10 right: reaction bed after 35 cycles; left: larger agglomerates after loosening of the bed

3.4 Summary of experimental results and implications for the process application

The superheated steam cycle is a well-established thermodynamic cycle for power generation. Different configurations and power sizes are readily available on the market. From today's perspective the maximum process temperature is in general limited to 600 °C due to economic reasons: The operation at higher temperatures demands more expensive alloys for the plant components and the higher costs are not compensated by the higher cycle efficiency. Market availability and scalability of the power cycle, the suitable temperature range as well as the working fluid water vapour (which is also required for the operation of the storage) lead to the conclusion that Rankine cycles powered by calcium oxide and water as the only energy source is one promising application.

Particular relevant operating condition is the discharge at pressures of 200 to 470 kPa in order to meet the upper temperature level of the current cycles of 545 - 600 °C. However the operation at these high pressures also requires a heat source with a temperature level of 120 - 150 °C to supply the discharge steam. In general thermal energy at this temperature level can usefully be incorporated into the process while at the same time thermal energy at a lower temperature level needs to be rejected from the Rankine cycle (e. g. condensation to the ambient). For the overall storage efficiency it could be highly valuable to make use of this low grade thermal energy to supply steam for the discharge procedure. For this reason the thermal discharge of the reaction system at pressures between 4 and 50 kPa, corresponding to evaporation temperatures between 30 and 81.3 °C has been additionally examined in the experimental section.

The experiments A-C showed that the discharge at pressures between 200 and 470 kPa achieved very good performances. For the first time a discharge temperature of 600 °C and 565 °C under significant

cooling loads of the heat transfer fluid was demonstrated. In all experiments even with drastically increased cooling loads the reaction proceeded close to the theoretical equilibrium temperature. It can be summarized that in this operating range reactors with high power densities can be designed to operate with discharge temperatures very close to the theoretical equilibrium temperature. Finally it was demonstrated that if the reaction system is operated at 470 kPa it is capable to supply thermal energy at a temperature of 600°C, the current maximum temperature of superheated steam cycles.

The thermal discharge at a pressure of 10 kPa was investigated due to its high relevance for a more efficient operation of a Rankine steam cycle (10 kPa is a common condensation pressure for dry cooling power plants). The experiments revealed that at this low pressure the equilibrium temperature was not reached in a technically relevant time. In the reactor a discharge temperature of 360 °C (in contrast to 400 °C equilibrium temperature) was determined for high cooling loads. Comparable limitations could be observed for all other investigated discharge pressures below 50 kPa. Overall it could be demonstrated that it is possible to discharge the storage reactor at reasonable reaction rates and vapour pressures between 4 and 50 kPa. However, in this operating range it is particular important that depending on the required thermal power an additional gap to the equilibrium temperature needs to be taken into account which reduces the achievable discharge temperature. Nevertheless even for the relatively low vapour pressures of 4 and 10 kPa outlet temperatures of 340 and 360 °C have been demonstrated (Fig. 7 and 8). These findings open the possibility of interesting interconnections between the steam cycle and the storage which will be thermodynamically analysed in chapter 4.3.

4 Evaluation of process integration based on molten salt CSP

For the study we consider the boundary conditions of a current molten salt tower plant [10]. The heat transfer fluid is a molten salt mixture (60% $NaNO_3$ + 40% KNO_3) operating in a temperature range from 290 °C to 565 °C. Even though the molten salt cycle is not the most innovative CSP concept discussed in the literature it has been chosen for a first reference integration scenario. The analysis should therefore be seen as one exemplarily process integration study to identify the general challenges related to the process integration of the calcium hydroxide system. Molten salt has been chosen due to the following reasons: The technology is commercially available and the community seeks for solutions to replace the expensive salt as the storage material. Additionally the coupling of the calcium hydroxide system with a superheated steam cycle offers potential synergies since water vapour is the working fluid in the cycle as well as the required reaction gas of the storage system. For the charging procedure we used available data for a central receiver power plant provided by DLR Institute of Solar Research. For the discharge procedure a state of the art power block configuration is considered.

Special focus in this chapter lies on the analysis of the discharge period of the storage where the power block should run only with thermal energy supplied by the storage system. During this discharging process it is particular important to consider the source of thermal energy required for evaporation since it represents a large share of the energy released by the reaction. Therefore

different configurations, including the extraction of low grade heat from the steam cycle, and their effect on the overall storage efficiency have been analysed.

During the charging period the temperature of the available heat sink for condensation of the reaction gas has huge influence on the amount of potentially stored thermal energy. Therefore the charging performance is evaluated against a commercial CPS plant technology based on a direct molten salt storage system.

4.1 Integration concept for CSP plant

For an application in CSP plants large storage capacities of up to 15 hours of nominal thermal power are desirable in order to ensure a continuous operation of the plant during most of the year. For a typical configuration with a nominal thermal power of 300 $MW_{thermal}$ this leads to a required storage capacity of 4500 MWh which corresponds to 11250 tons of calcium hydroxide. Taking these numbers into account it becomes obvious that for such large storage capacities the only economically viable way to realize indirectly heated reactors is the separation of power and capacity. In such a concept the heat exchanger is detached from the mass of the storage material. This allows to design the heat exchanger in respect to the required power level (the major cost) while the storage material can be stored in inexpensive tanks. Recently such an indirectly heated moving bed concept has been experimentally demonstrated in pilot scale [38]. The operation revealed that the gravity assisted flow of the storage material under energy efficient reaction conditions in the reactor is challenging and therefore currently under further investigation. Figure 11 shows the process scheme of a possible integration of a moving bed reactor concept into a CSP plant configuration.

During solar operation the heat transfer fluid delivers at first the nominal thermal load to the power block. As soon as the thermal power at the central receiver exceeds the demand of the power block the excess mass flow is directed into the thermochemical reactor. At this point a corresponding mass flow of $Ca(OH)_2$ is directed into the reactor. Heat is transferred to drive the endothermal reaction. CaO particles leave the reactor and are transported to a second storage container. Simultaneously water vapour is freed in the reaction chamber. To keep the reaction running, the water vapour must continuously be removed from the reactor which in turn demands a heat sink (e. g. ambient) to release the heat of condensation.

During non-solar hours the power block should ideally be continuously driven by the storage system. Therefore CaO is introduced into the reactor and additional water vapour needs to be supplied to drive the exothermal reaction. The discharge reaction temperature should be high enough to reach the maximum possible temperature of the heat transfer fluid of 565 °C in order to allow continuous operation of the power block at its nominal conditions. Obviously, an additional heat source is required to supply the enthalpy of evaporation for the discharge steam.

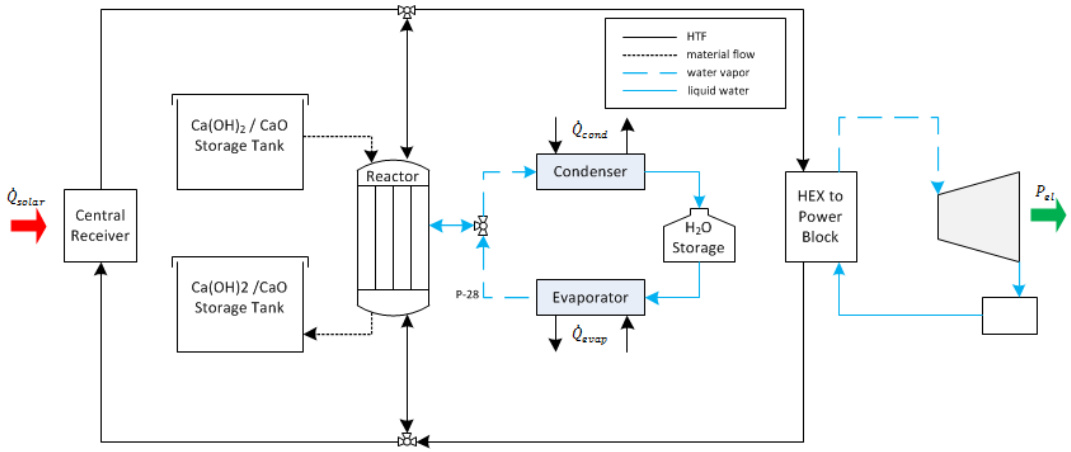

Fig. 11 Conceptual process design of an indirectly heated thermochemical reactor in a CSP plant configuration

4.2 Solar charging of the storage system

To charge the storage system integration into the molten salt cycle parallel to the central receiver is proposed (compare Fig. 11). However in this configuration the amount of thermal energy which can be incorporated into the storage system is limited due to the opposed characteristic of the thermochemical system and the sensible heat transfer fluid. While for the fluid the amount of transferred thermal energy is proportional to the change in temperature, the thermochemical system absorbs the enthalpy of reaction at a constant temperature level. As a consequence only the temperature difference above the reaction temperature can be used to charge the storage system. The temperature level of the reaction in turn depends on the condensation pressure thus on the specific boundary conditions of the plant. In order to reach the lowest possible reaction temperature, in this study we assume that the heat of condensation is released to the ambient.

By means of simple energy balances the mass flow of molten salt which is directed to the thermochemical reactor is calculated and the thermal power provided to the storage is calculated by the equation:

$$\dot{Q}_{TCS-charging} = \dot{m}_{salt} * cp_{salt} * (T_{inlet} - T_{reaction}) = \dot{n} \quad * \Delta H_{Reaction} \qquad (9)$$

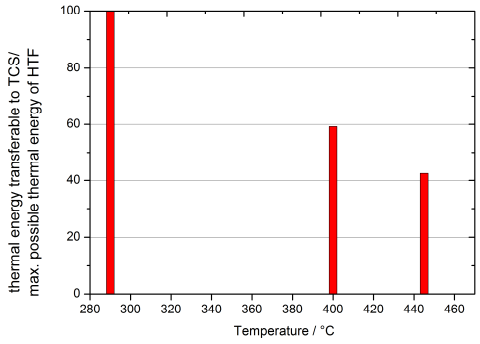

Fig. 12 Amount of stored thermal energy for different outlet temperatures at the thermochemical reactor

Figure 12 shows the percentage amount of stored thermal energy for two different conditions: an outlet temperature at the TCS reactor of 445 °C and of 400 °C. The reference value (100 %)

corresponds to the direct storage of the molten salt in a two tank system. The value of 400 °C corresponds to the thermodynamic minimum temperature that can be calculated according to Barin [35] for a given pressure of 10 kPa. It becomes obvious that at this theoretical minimal outlet temperature of 400 °C, only 59 % of the amount of stored energy in the molten salt tanks can be reached with the thermochemical system. According to our experimental investigation of the commercial $Ca(OH)_2$ (please refer to [36]), the reaction rate at such low pressures limits additionally the practical operation window of the reaction. If a more realistic outlet temperature of 445 °C is considered only 42 % of the possible amount of thermal energy can be stored. Or, expressed in alternative values: whereas in a direct molten salt system 10 h of nominal thermal load are stored the investigated thermochemical storage system can theoretically only be charged with 5.9 hours of nominal thermal load and 4.2 hours for the more realistic case of an outlet temperature of 445 °C.

This can be contributed to two reasons: one is that the minimal condensation temperature of the plants location limits the temperature difference between the maximum temperature of the heat transfer fluid and the temperature level of the reaction. The second is that kinetic limitations at such low vapour pressure enforce an additional temperature difference of approximately 45 K to the theoretical reaction temperature (which has been experimentally identified in [19]). This drastic difference makes it obvious that a thermochemical storage cannot simply substitute a conventional storage method without changing at least some parts of the overall concept.

However, if the configuration of the plant will be adapted to the storage system the pointed out problems can be overcome. One proposal with minimal adaptation of the CSP technology would be to have two different central receivers. One receiver would still operate in the nominal temperature range of the power block from 290 - 565 °C to supply the power block during on sun operation. The second receiver cycle would be especially designed to charge the storage system during daytime and operate at temperatures between 565 °C and 445 °C. Of course the higher return temperature of the heat transfer fluid provokes higher losses in the central receiver. Nevertheless a detailed simulation of such a configuration could be worth investigating.

4.3 Power generation driven by the storage system – operation modes

The steam cycle for power generation considered in this work is based on a standard Rankine cycle configuration for molten salt solar tower plans. The configuration consists of two high pressure turbine stages, one reheater, and 5 low pressure turbine stages. Live steam is generated at 136000 kPa and 552 °C Steam is extracted at 6 turbine stages to preheat the feed water. The cycle is designed for a nominal output of 125 MW_{el} and reaches a gross efficiency of 0.419 at a condensation pressure of 10 kPa. Table 2 summarizes the main nominal parameters of the power block.

Table 2 *Nominal values for power block cycle*

HTF Parameters	
Nominal Thermal Input / MW_{th}	298.35
Flowrate of HTF / (kg/s)	713.373
HTF Inlet Temperature / °C	565
HTF Return Temperature/ °C	290
Steam Parameters	
Live Steam Flowrate / (kg/s)	384.451
Live/Reheat Steam Pressure / kPa	13600/3200

Live/Reheat Steam Temperature / °C	334/552

Turbine parameters	
Gross Turbine Power / $MW_{electric}$	125
Turbine Isentropic Efficiency / %	86
Generator Efficiency/ %	96
Power Block Gross Efficiency / %	41.9

Condenser	
Condensation Pressure / kPa	10

Steam Extraction	
(EXP1) – Pressure/kPa / Flowrate/(kg/s)	5000 / 2.8
(EXP2) – Pressure/kPa / Flowrate/(kg/s)	3400 / 10.9
(EXP3) – Pressure/kPa / Flowrate/(kg/s)	1000 / 5
(EXP4) – Pressure/kPa / Flowrate/(kg/s)	450 / 5.3
(EXP5) – Pressure/kPa / Flowrate/(kg/s)	150 / 4.9
(EXP6) – Pressure/kPa / Flowrate/(kg/s)	40 / 3.7

Thermal Power	
Superheater / MW	89.796
Reheater / MW	41.202
Steam Generator / MW	114.47
Preheater / MW	52.89

Four different operation strategies where the steam cycle is only powered by the thermochemical storage system are analysed. The operation modes differ in the quality and flow rate of steam which is extracted at different turbine stages to supply vapour for the discharge reaction. For each operation mode the required flow rate at the extraction point is calculated by general mass and energy balances. The power block is simulated with the commercial software tool Ebsilon©. By means of the simulation the electrical output in part load mode for the different steam extraction flow rates is determined.

Figure 13 shows the process flow diagram of the steam cycle and the operation of the thermochemical reactor(s) during the discharge procedure. We at first describe the different configurations while in the subsequent section the overall storage efficiencies are compared.

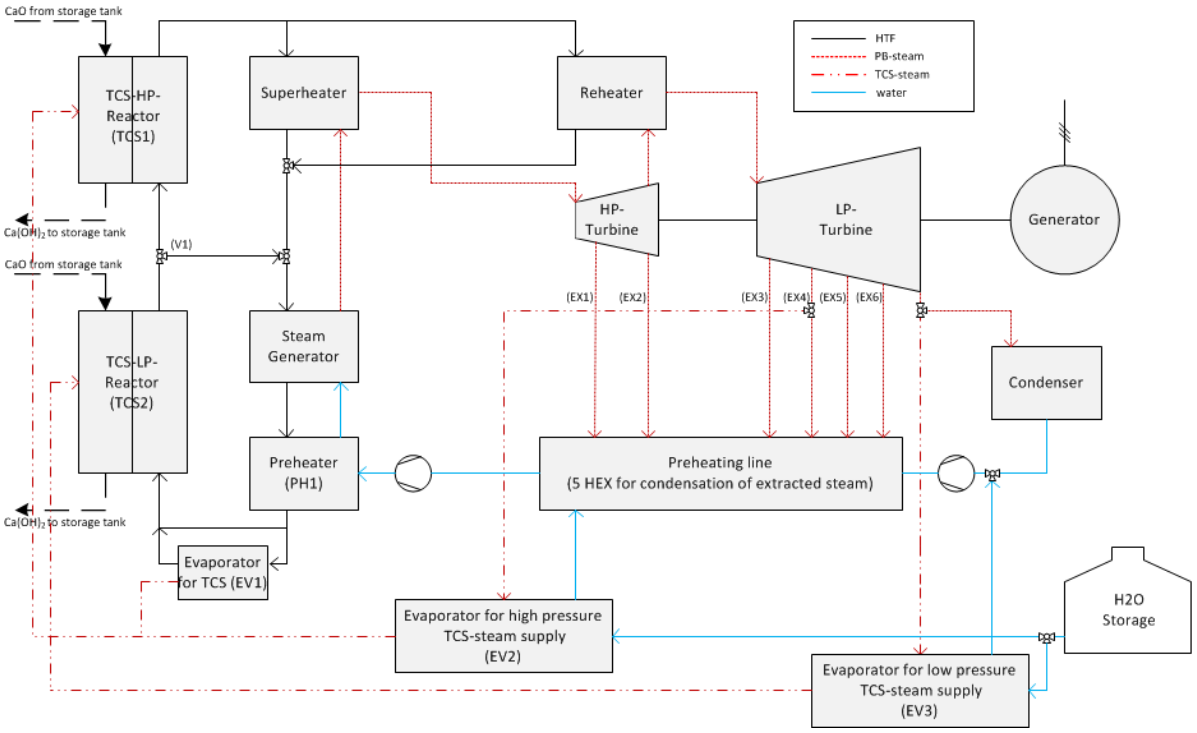

Fig. 13 Flow sheet of power block operation with the thermochemical storage system

A - reference case

In the reference case only the high pressure TCS-Reactor (TCS1) and the evaporator (EV1) are in operation. Discharge steam is generated in evaporator (EV1) which is driven by thermal energy supplied by the heat transfer fluid. The molten salt is directed to evaporator (EV1) after it leaves the preheater with an outlet temperature of 290 °C. The steam is generated at a pressure of 470 kPa and directed into the reactor (TCS1). As we demonstrated in the experimental section (compare Fig. 4) with the operation at 470 kPa a reaction temperature of 600 °C can be expected. Therefore the power block can continue to operate at nominal conditions of 552 °C superheated steam.

In this operation mode the reactor not only has to supply the nominal thermal power of the steam cycle but also the thermal power for the evaporation of the required discharge steam (compare Fig. 13). The required discharge power can thus be calculated by the equations:

$$\dot{Q}_{TCS-discharging-A} = \dot{Q}_{PB_{nominal}} + \dot{Q}_{evaporation} \qquad (1)$$

$$\dot{n} * \Delta H_{reaction} = \dot{Q}_{PB_{nominal}} + \dot{n} * \Delta H_{evaporation(149.5°C,470\ kPa)} \qquad (2)$$

With the enthalpy values given in Table 3, the required thermal power that has to be delivered by the thermochemical reactor $\dot{Q}_{TCS-discharging-A}$ accounts to 470.16 MW in this operation mode.

Table 3 *General values for the calculations*

General Values	
$\dot{Q}_{PB_{nominal}}$ / MW	298.35
$\eta_{PBnominal}$	0.419
$\Delta H_{reaction}$ / (kJ/mol)	104
$\Delta H_{evaporation(149,5°C,470\ kPa)}$ / (kJ/mol)	38

M_{H2O} / (kg/mol)	0.018

B – Steam extraction at LP-Turbine

In operation mode B steam is extracted at the second stage of the low pressure turbine at extraction point 4 (EX4). The extracted steam is directed into evaporator (EV2) where steam at 450 kPa is generated for the thermochemical discharge reaction. Again according to our experimental demonstration in section 3.1 the reaction temperature at this pressure will be close to the equilibrium temperature (597 °C). For this simplified examination, losses related to the heat exchanger (EV2) are neglected. In contrast to operation mode A the thermal power required in this configuration is only the nominal thermal power of the power block (298.35 MW). Thus the molar rate of reaction can be calculated by the equation:

$$\dot{Q}_{TCS-discharging-B} = \dot{Q}_{PB_{nominal}} = \dot{n} * \Delta H_{reaction} \qquad (3)$$

With the molar rate of reaction the flow rate of required water vapour for the discharge reaction can be calculated by equation 4:

$$\dot{m}_{vapor} = \dot{n} * M_{H2O} \qquad (4)$$

and accounts 51.68 kg/s. Consequently, this amount of steam is not available for power generation. Therefore, the operation of the power block is simulated with a steam extraction of 51.68 kg/s at (EX4) which results in a reduced electrical output of 92.1 MW compared to the nominal output of 125 MW (no steam is extracted for the TCS operation).

C – Steam extraction at LP-Turbine and use of exhaust steam

In order to further increase the efficiency it seems reasonable to make use of the condensation enthalpy of the exhaust steam at the outlet of the low pressure turbine. Nevertheless this operation mode results in a more complex integration. To incorporate the steam at the condensation pressure of 10 kPa the outlet flow of the low pressure turbine is partially directed to evaporator (EV3). There steam is generated at a pressure of 10 kPa and directed into a second reactor (TCS2) for low pressure operation. Losses of the heat exchanger (EV3) are again neglected. In this operation mode two reactors are necessary because the temperature level which is reached in TCS2 is limited. Taking the experimental results for the discharge at 10 kPa into account (compare Fig. 8) a temperature of around 360 °C can be expected. Since the steam generator of the plant operates at 334 °C, the low pressure reactor TCS2 is in principle able to supply the thermal energy for the steam generator and the preheater. Consequently, only the superheater and the reheater need to be driven by TCS1. Therefore the mass flow of the HTF is separated after TCS2 at valve (V1). One part is directed to supply the steam generator and the preheater whereas a smaller mass flow is directed into TCS1. The reactor TCS1 again operates at 450 kPa while, like in operation mode B, the required steam comes from evaporator EV2 which in turn is driven by condensation of steam from extraction point 4 (EX4). Since TCS1 now only provides the thermal power required by the superheater and the reheater the necessary thermal power is clearly reduced:

$$\dot{Q}_{TCS1-discharging-C} = \dot{Q}_{superheater} + \dot{Q}_{reheater} = \dot{n}_{TCS1-C} * \Delta H_{reaction} \qquad (5)$$

Accordingly the necessary steam flow rate at (EX4) is calculated to 22.69 kg/s. The molar reaction rate required at TCS2 is calculated by:

$$\dot{Q}_{TCS2-discharging-C} = \dot{Q}_{evaporator} + \dot{Q}_{preheater} = \dot{n}_{TCS2-C} * \Delta H_{reaction} \quad (6)$$

According to equation 4 the flow rate of steam which needs to be generated by the enthalpy of condensation at 10 kPa is calculated to 28.99 kg/s. Since in this case, a huge fraction of the reaction gas could be derived from the condensation pressure of the power block, the calculated electrical output for this configuration is 109.91 MW.

D - Steam extraction at LP-Turbine and lowering of condensation temperature

In operation mode D it is assumed that the TCS2 reactor operates at a vapour pressure of 4 kPa, which in principle would allow to reduce the condensation temperature of the power block. However, it is obvious that operating the system at such low pressures requires huge efforts in gas handling and heat exchange. The experimental results presented in fig. 7 show that a reaction temperature of 340 °C can be reached which is in principle high enough to supply the steam generator and the preheater (comparable to configuration C). Since evaporator (EV3) operates at a pressure of 4 kPa (instead of 10 kPa) the efficiency of the power block is increased which could partially compensate the reduced mass flow of steam. However, this configuration would require an additional turbine stage in which 28.99 kg/s of steam can be condensed at 4 kPa while 24.7 kg/s are condensed at 10 kPa after the nominal fifth turbine stage (configuration is not illustrated in Fig. 13). Comparable to operation mode C an additional mass flow of 22.69 kg/s of steam must be extracted at 450 kPa at (EX4) to supply the TCS1 reactor. The calculated power output of this configuration is 112.48 MW which is only slightly higher than case C that could be realized with clearly minor changes of the power block.

4.4 Storage efficiency

Table 4 summarizes the results for the different operation modes. It becomes obvious that in the reference case A the power block operates at its nominal electric output but at the same time the thermal power required at the thermochemical reactor is much higher compared to the configurations where steam is extracted from the power block.

Table 4 *Calculated thermal Power, flow rates of extracted steam and electrical output of the power block for the different operation modes*

Mode	$\dot{Q}_{TCS1}$ / MW$_{th}$	$\dot{Q}_{TCS2}$ / MW$_{th}$	$\dot{m}_{vapor}$@(EX4) /(kg/s)	$\dot{m}_{vapor}$@(EV3) /(kg/s)	P_{el} /MW$_{el}$
A	470.16	0	0	0	125
B	298.35	0	51.68	0	92.1
C	130.99	167.376	22.69	28.99	109.91
D	130.99	167.376	22.69	28.99	112.484

Therefore, in order to be able to compare the operation modes we defined an efficiency which relates the electric energy output during discharge of the storage to the potential electricity which has not been produced during the charging period of the storage system. The efficiency is represented by equation 7:

$$\eta_{storage} = \frac{P_{el\ discharging-case\ A-D}}{\dot{Q}_{TCS-charging-case\ A-D} * \eta_{PBnominal}} \quad (7)$$

Further we assume that for all cases the thermal power required during discharge is equal to the thermal power supplied during the charging procedure:

$$\dot{Q}_{TCS-charging-case\ A-D} = \dot{Q}_{TCS1-\ discharging-\ case\ A-D} + \dot{Q}_{TCS2-\ discharging-\ case\ A-D} \quad (8)$$

Consequently since losses are neglected the ratio of charging power to discharging power is 1 and the storage can be discharged exactly for the time span as it was charged.

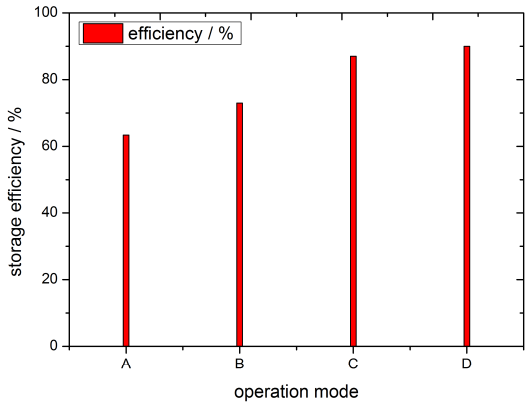

Fig. 14 *Storage efficiency according to equation 7 and 8 for the different operation modes*

Figure 14 shows the storage efficiency calculated by equation 7 and 8 for the different configurations. The reference case A only reaches an efficiency of 63.4 %. The low efficiency can be mainly attributed to the fact that the energy content of the steam released during the charging process is not used and the steam required for the discharge needs to be generated by thermal energy from the storage itself. Therefore we lose roughly 36 % of the energy content which is related to the ratio of enthalpy of condensation to the enthalpy of reaction (38/104 (kJ/mol)).

In operation mode B a large steam mass flow needs to be extracted at 450 kPa from the low pressure turbine. This clearly reduces the electrical output of the power block. But on the other hand the thermal power required from the storage during the discharging process is also reduced compared to the reference case A. Overall we reach a clearly increased storage efficiency of 73 %. Advantageous of this concept is that only one TCS reactor is required and it is operated at a relatively high pressure. The higher pressure in principal allows smaller pipe diameters and compact reactor designs. Additionally, as experimentally demonstrated (compare chapter 3.1), a reaction pressure of >200 kPa allows for outlet temperatures that are very close to the equilibrium even for high required reaction rates.

Operation mode C greatly improves the overall efficiency to 87 %. In this operation mode only the amount of thermal power required at the higher temperature level of 565 °C is generated in TCS1. The remaining required thermal power is generated in TCS2 where steam which has no exergetic value in the steam cycle is used for the discharging reaction. Consequently a much smaller mass flow of steam has to be extracted at point 4 (EX4) which in turn increases the electricity output. The obvious disadvantage of this operation mode is that in total four devices are necessary: two TCS-

reactors and two evaporators. The direct incorporation of the extracted steam from the turbines to the thermochemical reactors (to avoid the two evaporators) is to our knowledge not possible. The steam which was in contact with the storage material might not be clean enough anymore to operate the turbines. Additionally the operation of the thermochemical reactor at such a low vapour pressure of 10 kPa might be challenging due to: large pipe diameters that are required for the transport of the steam. Furthermore the reactor design becomes more complex since the reaction gas distribution within the reaction bed is easier for higher pressures. And finally, the reaction temperature which can be reached at this vapour pressures deviates clearly from the theoretical value if technical relevant reaction rates are required (compare Fig. 8).

Operation mode D reaches an efficiency of 90 %. But since this increase of the electrical output of the power block would lead to even more challenging operating conditions of the power block and the storage, it is doubtful that the increase of 3 percentage points in storage efficiency will be economically reasonable.

To summarize: the experimental investigation of commercially available $Ca(OH)_2$ shows that in principle the required heat sink of the power block (cooling tower) could be combined with the required low grade heat source of the thermochemical system (evaporator). This concept clearly improves the overall efficiency of the thermochemical storage but requires at the same time to a certain extent modifications of the power block. The simplest configuration reaches a storage efficiency of 73 % (in comparison 63,4 % for the baseline case) while with a more complex and technically challenging integration values of 87 % and more could be reached. It has to be stated that for all operation modes with increased efficiency (mode B, C and D) a large fraction of the nominal steam mass flow has to be extracted at the low pressure turbine. Such a large steam extraction is thermodynamically possible but to the knowledge of the author´s no turbine, which allows such an operation, is currently available on the market. The design of such a turbine is technically challenging and thus would demand extensive development work. One possibility to overcome this challenge might be to use two separated turbines especially designed for the required boundary conditions instead of extracting a large steam fraction from one low pressure turbine stage.

To which extend the released steam during the charging of the storage can be used to increase the efficiency of the power block and compensates for the reduced power output during the discharging process needs to be evaluated based on a more detailed simulation of the plant including economic aspects.

5 Conclusions

In this study the thermal discharging of the reaction of CaO and water vapour has been experimentally demonstrated in lab scale in the complete temperature (280 °C - 600 °C) and pressure (4 – 470 kPa) range which is relevant to operate a Rankine steam cycle with the thermochemical storage system. The experiments revealed that especially at pressures of 200 kPa and more the reaction is very fast even at the (or very close to the) equilibrium temperature. Therefore it can be concluded that for this pressure range reactors can be designed to operate with high power densities and at outlet temperatures close to the equilibrium temperature. The discharge procedure at pressures between 4 and 50 kPa has also been experimentally demonstrated and showed promising performance. Nevertheless at this low pressure operation an additional temperature difference to the equilibrium temperature occurs and has to be maintained if the reactor should be operated at

high power densities. With the presented discharge experiments and our previously published charging experiments the complete relevant operating range of the thermochemical storage system has been experimentally characterised in lab scale. The experimental results now provide a more realistic understanding of the operation characteristic as well as the quantification of achievable charge and discharge temperatures. Based on this knowledge the applicability of the storage for many real processes can now be assessed more accurate from a technical as well as a thermodynamic point of view.

Besides the experimental investigations a first study on the integration of the thermochemical system in a conventional CSP plant has been thermodynamically analysed. It could be shown that, when the steam production required during discharge is thermally integrated into the Rankine steam cycle a high storage efficiency of 87 % can be reached. However the charging procedure with molten salt as the heat transfer fluid is challenging: The minimal condensation pressure of 10 kPa available at most CSP locations (dry cooling in hot regions) as well as kinetic limitations at low pressure charging enforce reaction temperatures of 445 °C or higher. In conclusion the thermal power which can be incorporated is limited due to the small temperature difference between the reaction temperature and today's maximum operating temperature of the salt. On the other hand the experimentally demonstrated characteristic of the storage system indicate promising potential for a wide range of applications. The posed charging challenge can be overcome by using heat transfer fluids which allow a higher maximum temperature, for example liquid metal. Another approach to charge the storage system would be direct solar irradiation in a particle receiver. The determined potentially achievable high storage efficiencies indicate that such applications should be investigated in future studies.

Nomenclature

CSP	Concentrated Solar Power
cp	specific heat capacity
EV	evaporator
EX	extraction point
F	filling level
HEX	heat exchanger
HTF	heat transfer fluid
LP	low pressure
PH	preheater
P	electrical power output
p	pressure
TCS	thermochemical system
T	temperature
V	valve
ϑ	temperature measurement point, thermocouple
X_{tot}	conversion
%w	weight percentage
d_{50}	median diameter of the particle size distribution
$\dot{V}$	volume flow
$\dot{Q}$	thermal power output
$\dot{n}$	molar rate of reaction
$\dot{m}$	mass flow rate
η	efficiency
ΔH	enthalpy change
M_{H2O}	molar mass

References

[1] Zhang HL, Baeyens J, Degrève J, Cacères G. Concentrated solar power plants: Review and design methodology. Renew Sustain Energy Rev 2013;22:466–81. doi:10.1016/j.rser.2013.01.032.

[2] Dunn RI, Hearps PJ, Wright MN. Molten-Salt Power Towers: Newly Commercial Concentrating Solar Storage. Proc IEEE 2012;100:504–15. doi:10.1109/JPROC.2011.2163739.

[3] Franchini G, Perdichizzi A, Ravelli S, Barigozzi G. A comparative study between parabolic trough and solar tower technologies in Solar Rankine Cycle and Integrated Solar Combined Cycle plants. Sol Energy 2013;98:302–14. doi:10.1016/j.solener.2013.09.033.

[4] IRENA. Renewable Energy Technologies: Cost Analysis Series Concentrating Solar Power. IRENA Work Pap 2012.

[5] Kuravi S, Trahan J, Goswami DY, Rahman MM, Stefanakos EK. Thermal energy storage technologies and systems for concentrating solar power plants. Prog Energy Combust Sci 2013;39:285–319. doi:10.1016/j.pecs.2013.02.001.

[6] Flueckiger SM, Iverson BD, Garimella S V. Economic Optimization of a Concentrating Solar Power Plant With Molten-Salt Thermocline Storage. J Sol Energy Eng 2013;136:1–8. doi:10.1115/1.4025516.

[7] Xu Y, Ren Q, Zheng Z-J, He Y-L. Evaluation and optimization of melting performance for a latent heat thermal energy storage unit partially filled with porous media. Appl Energy 2017;193:84–95. doi:10.1016/j.apenergy.2017.02.019.

[8] Zhou L, Xu G, Zhao S, Xu C, Yang Y. Parametric analysis and process optimization of steam cycle in double reheat ultra-supercritical power plants. Appl Therm Eng 2016;99:652–60. doi:10.1016/j.applthermaleng.2016.01.047.

[9] Meng ZN, Zhang P. Experimental and numerical investigation of a tube-in-tank latent thermal energy storage unit using composite PCM. Appl Energy 2017;190:524–39. doi:10.1016/j.apenergy.2016.12.163.

[10] Liu M, Steven Tay NH, Bell S, Belusko M, Jacob R, Will G, et al. Review on concentrating solar power plants and new developments in high temperature thermal energy storage technologies. Renew Sustain Energy Rev 2016;53:1411–32. doi:10.1016/j.rser.2015.09.026.

[11] Zhang H, Baeyens J, Cáceres G, Degrève J, Lv Y. Thermal energy storage: Recent developments and practical aspects. Prog Energy Combust Sci 2016;53:1–40. doi:10.1016/j.pecs.2015.10.003.

[12] Miró L, Gasia J, Cabeza LF. Thermal energy storage (TES) for industrial waste heat (IWH) recovery: A review. Appl Energy 2016;179:284–301. doi:10.1016/j.apenergy.2016.06.147.

[13] Gil A, Medrano M, Martorell I, Lázaro A, Dolado P, Zalba B, et al. State of the art on high temperature thermal energy storage for power generation. Part 1—Concepts, materials and modellization. Renew Sustain Energy Rev 2010;14:31–55.

[14] Medrano M, Gil A, Martorell I, Potau X, Cabeza LF. State of the art on high-temperature thermal energy storage for power generation. Part 2—Case studies. Renew Sustain Energy Rev 2010;14:56–72.

[15] Cabeza LF, Solé A, Fontanet X, Barreneche C, Jové A, Gallas M, et al. Thermochemical energy

storage by consecutive reactions for higher efficient concentrated solar power plants (CSP): Proof of concept. Appl Energy 2017;185:836–45. doi:10.1016/j.apenergy.2016.10.093.

[16] Chacartegui R, Alovisio A, Ortiz C, Valverde JM, Verda V, Becerra JA. Thermochemical energy storage of concentrated solar power by integration of the calcium looping process and a CO 2 power cycle. Appl Energy 2016;173:589–605. doi:10.1016/j.apenergy.2016.04.053.

[17] Deutsch M, Müller D, Aumeyr C, Jordan C, Gierl-Mayer C, Weinberger P, et al. Systematic search algorithm for potential thermochemical energy storage systems. Appl Energy 2016;183:113–20. doi:10.1016/j.apenergy.2016.08.142.

[18] Aydin D, Casey SP, Riffat S. The latest advancements on thermochemical heat storage systems. Renew Sustain Energy Rev 2015;41:356–67. doi:10.1016/j.rser.2014.08.054.

[19] Pardo P, Deydier A, Anxionnaz-Minvielle Z, Rougé S, Cabassud M, Cognet P. A review on high temperature thermochemical heat energy storage. Renew Sustain Energy Rev 2014;32:591–610. doi:10.1016/j.rser.2013.12.014.

[20] Prieto C, Cooper P, Fernández AI, Cabeza LF. Review of technology: Thermochemical energy storage for concentrated solar power plants. Renew Sustain Energy Rev 2016;60:909–29. doi:10.1016/j.rser.2015.12.364.

[21] Rosemary JK, Bauerle GL, Springer TH. Solar Energy Storage Using Reversible Hydration-Dehydration of CaO-Ca(OH)2. J Energy 1979;3:321–2. doi:10.2514/3.62440.

[22] Schaube F, Koch L, Wörner A, Müller-Steinhagen H. A thermodynamic and kinetic study of the de- and rehydration of Ca(OH)2 at high H2O partial pressures for thermo-chemical heat storage. Thermochim Acta 2012;538:9–20. doi:10.1016/j.tca.2012.03.003.

[23] Criado YA, Alonso M, Abanades JC. Kinetics of the CaO/Ca(OH) 2 Hydration/Dehydration Reaction for Thermochemical Energy Storage Applications. Ind Eng Chem Res 2014;53:12594–601. doi:10.1021/ie404246p.

[24] Galwey AK, Laverty GM. A kinetic and mechanistic study of the dehydroxylation of calcium hydroxide. Thermochim Acta 1993;228:359–78. doi:10.1016/0040-6031(93)80304-S.

[25] Nagel T, Shao H, Roßkopf C, Linder M, Wörner A, Kolditz O. The influence of gas–solid reaction kinetics in models of thermochemical heat storage under monotonic and cyclic loading. Appl Energy 2014;136:289–302. doi:10.1016/j.apenergy.2014.08.104.

[26] Wang W, Kolditz O, Nagel T. Parallel finite element modelling of multi-physical processes in thermochemical energy storage devices. Appl Energy 2016. doi:10.1016/j.apenergy.2016.03.053.

[27] Kariya J, Ryu J, Kato Y. Development of thermal storage material using vermiculite and calcium hydroxide. Appl Therm Eng 2016;94:186–92. doi:10.1016/j.applthermaleng.2015.10.090.

[28] Shkatulov A, Ryu J, Kato Y, Aristov Y. Composite material “Mg(OH)2/vermiculite”: A promising new candidate for storage of middle temperature heat. Energy 2012;44:1028–34. doi:10.1016/j.energy.2012.04.045.

[29] Afflerbach S, Kappes M, Gipperich A, Trettin R, Krumm W. Semipermeable encapsulation of calcium hydroxide for thermochemical heat storage solutions. Sol Energy 2017;148:1–11. doi:10.1016/j.solener.2017.03.074.

[30] Pardo P, Anxionnaz-Minvielle Z, Rougé S, Cognet P, Cabassud M. Ca(OH)2/CaO reversible reaction in a fluidized bed reactor for thermochemical heat storage. Sol Energy

2014;107:605–16. doi:10.1016/j.solener.2014.06.010.

[31] Criado YA, Alonso M, Abanades JC, Anxionnaz-Minvielle Z. Conceptual process design of a CaO/Ca(OH)2 thermochemical energy storage system using fluidized bed reactors. Appl Therm Eng 2014;73:1085–92. doi:10.1016/j.applthermaleng.2014.08.065.

[32] Rougé S, A. Criado Y, Soriano O, Abanades JC. Continuous CaO/Ca(OH) 2 Fluidized Bed Reactor for Energy Storage: First Experimental Results and Reactor Model Validation. Ind Eng Chem Res 2017;56:844–52. doi:10.1021/acs.iecr.6b04105.

[33] Ogura H, Yamamoto T, Kage H, Matsuno Y, Mujumdar AS. Effects of heat exchange condition on hot air production by a chemical heat pump dryer using CaO/H2O/Ca(OH)2 reaction. Chem Eng J 2002;86:3–10. doi:10.1016/S1385-8947(01)00265-0.

[34] Yan J, Zhao CY. Experimental study of CaO/Ca(OH)2 in a fixed-bed reactor for thermochemical heat storage. Appl Energy 2016;175:277–84. doi:10.1016/j.apenergy.2016.05.038.

[35] Barin I. Thermochemical Data of Pure Substances. Weinheim, Germany: Wiley-VCH Verlag GmbH; 1995. doi:10.1002/9783527619825.

[36] Schmidt M, Gutierrez A, Linder M. Thermochemical energy storage with CaO/Ca(OH)2 – Experimental investigation of the thermal capability at low vapor pressures in a lab scale reactor. Appl Energy 2017;188:672–81. doi:10.1016/j.apenergy.2016.11.023.

[37] Samms JAC, Evans BE. Thermal dissociation of Ca(OH)2 at elevated pressures. J Appl Chem 2007;18:5–8. doi:10.1002/jctb.5010180102.

[38] Schmidt M, Gollsch M, Giger F, Grün M, Linder M. Development of a moving bed pilot plant for thermochemical energy storage with CaO/Ca(OH)2. SOLARPACES 2015 Int. Conf. Conc. Sol. Power Chem. Energy Syst., vol. 1734, AIP Publishing; 2016, p. 50041. doi:10.1063/1.4949139.